Journal of Carcinogenesis
Covering Genesis to Therapeutics
Journal of Carcinogenesis, ISSN: 1477-3163
2025; Vol 24: Issue 4, https://carcinogenesis.com/

A Combination of Cross Domain Features for Face Recognition

Jyothi kiran G C[1], Ramachandra A C[2], Jagadeesh H S[3], K B Raja[4]

[1]Assistant Professor, Dept. of Electronics and Communication Engineering, BMS College, Bengaluru, India, jyothirkk1@gmail.com.

[2]Dept. of Electronics and Communication Engineering, NMIT, Bengaluru, India, ramachandra.ace@gmail.com

[3]Dept. of Electronics and Communication Engineering, Sir. MVIT, Bangalore

[4]Dept. of Electronics and Communication Engineering, University Visvesvaraya College of Engineering, Bangalore University, Bengaluru, India, raja_kb@yahoo.com

ABSTRACT

Face recognition in biometrics is a difficult process because of factors including individual differences in facial emotions, illumination, resolution, facial rotation, and facial structure similarities. "A Combination of Cross Domain Features for Face Recognition" is what we suggest here. The benchmarked face images are considered, downsized to consistent 128x128 dimensions, and converted to grayscale. Face photos are compressed, and their quality is improved by using the Discrete Wavelet Transform (DWT). Initial characteristics that are unaffected by changes in an image's lighting are extracted using the Histogram of Oriented Gradients (HOG) on a compressed LL band of DWT. By connecting the LL band's output to the HOG's input, the DWT and HOG's LL bands are connected in a cascade. HOG's input and output are combined to create new, strong final features. The system's results when comparing test and database features are calculated using the Euclidean Distance (ED). It has been noted that the suggested system outperforms the current ones in terms of results.

KEYWORDS: *Convolution, Discrete Wavelet Transform, Euclidean Distance, Face Recognition, HOG.*

How to Cite: Jyothi kiran G C, Ramachandra A C, Jagadeesh H S, K B Raja., (2025) A Combination of Cross Domain Features for Face Recognition, *Journal of Carcinogenesis, Vol.24, No.4*, 120-130.

1. INTRODUCTION

Because of their versatile appearance and wide range of postures, humans might be difficult to identify in a face photograph. In the context of the current global COVID-19 pandemic, facial recognition is a crucial tool for human-machine communication that allows for social distance to be maintained when using public transit, entering offices, and entering hospitals, among other settings. The main prerequisite is a robust feature collection that enables efficient human separation, even in face image backgrounds that are cluttered. As the most advanced method of computerized human identification, biometrics have been created since ancient times and have ushered in a new era of global security [1, 2, 3]. Both physiological characteristics, such as a face, palm print, fingerprint, or iris pattern, and behavioural characteristics, such as a signature, keystroke, or stride, are used to determine biometric credentials [4]. To extract characteristics for biometric recognition and to gain additional information for other applications, the temporal domain/spatial domain signals are transformed into other domains. Fourier Transform [5], Discrete Fourier Transform [6], Fast Fourier Transform [7, 8], and Discrete Cosine and Sine Transforms [9] are easily accessible transformations that convert the time domain/spatial domain into the frequency domain to extract the signal's frequency components without providing time information. The Wavelet Transform [10] solves the problem of the transformations' inability to provide frequency components that correlate to time and location. Electronic devices, banking, immigration, law enforcement, telecommunication networks, staff time and attendance tracking, cloud computing, big data analytics, video analytics, health care systems, national security systems, and numerous web-based applications are just a few of the many biometrics application areas. Contributions: We presented the cascade of DWT and HOG approaches for face image initial features in this research. The LL band of the DWT and HOG matrices, which are the most common and reliable features of face images for human recognition, are convolved to extract the final features. The effectiveness of the suggested approach is confirmed by comparing databases and identifying face picture features using the distance measure ED.

Organization: This is how the remainder of this research report is organized. Section II covers earlier research on face recognition feature extraction and classification methods. The suggested system model is covered in Section III. The

suggested algorithm is presented in Section IV, which also discusses the system's experimental findings and comparison with other methods. This paper is concluded with suggestions for further research in Section VI.

2. LITERATURE SURVEY

A single sample per person (SSPP) face recognition system was proposed by X. Han et al. [11]. The features are classified using SSPP using Pearson correlation and the histograms of oriented gradients (HOG) algorithm, which computes the features based on the face matrix structure. The model performs well because to the methods of HOG and Pearson correlation, which efficiently sort variations in faces. The use of HOG in feature extraction for face recognition was explained by Rajput et al. [12]. Images of faces in frontal poses with neutral expressions, normal lighting, and no occlusions are considered. An artist's drawing of the query face image is taken into consideration and used as the HOG feature descriptor. The KNN classifier is used to calculate the HOGs of artist sketches and relate them to the database's face photos. ZXie et al. [13] introduced a face recognition system that combines the Local Binary Pattern (LBP) and HOG. The LBP operator is employed to extract the texture feature of the face because the LBP has limitations when it comes to extracting the edge and direction information in face images. The HOG operator extracts the edge characteristics from the raw infrared facial photos. To get better features, texture and edge features are combined using Multiple Kernel Learning (MKL). Three key contributions were made by Ghorbani et al. [14] when they proposed HOG and LBP features for face recognition. Initially, the HOG descriptor is employed to minimize mistakes in face images caused by occlusions, pose, and variations in illumination. Second, the LBP is combined with HOG descriptors at various scales to capture essential structure for facial identification. Finding a better feature selection method to get rid of unnecessary and irrelevant features comes in third. For face recognition, H Wang et al. [15] proposed a combination of Local Difference Binary (LDB) and HOG. The local pattern characteristics of a facial image are extracted using the LDB descriptor. HOG extracts the edge features of the face images. The high quality of features is enhanced by the combination of LDB and HOG features. The ORL and Yale face databases are used to test the experimental results. To concatenate various feature sources for a facial image, Nhat and Hoang [16] created a fusion of feature sets based on canonical correlation analysis. Features based on block division are extracted using standard descriptors like LBP, HOG, and GIST.

The methods for identifying anxiety in three classes—neutral, low stress, and high stress—from facial frontal images were put out by Prasetio et al. [17]. Three components make up the face image: the lips, nose, and pairs of eyes. Each pair of images has its features extracted using DoG, HOG, and DWT. The RICA measures the strength of orthonormality traits. The nonlinear covariance is distributed via the GDA. ConvNet's depth-based learning uses the picture pairs' histogram characteristics to test the model. Detecting faces in any image, extracting features from the eyes and lips, and classifying them into six emotions—happy, fear, anger, disgust, neutral, and sadness—are the goals of Jain et al. [18]. To improve data classification, techniques such applying a Gabor filter to the training images or using HOG and DWT are used. Passing the training images through HOG and then SVM produced a better result. A nibble-based face recognition method utilizing convolution of hybrid features was proposed by Rangsee et al. [19]. To improve computational performance, a new method of transforming each pixel's decimal value into 8-bit binary and splitting it into Left-Side Nibble (LSN) and Right-Side Nibble (RSN) is presented. A decimal value ranging from 0 to 240 is substituted for the 4-bit LSN. Only the LL band coefficients are assessed as the initial set of transform domain features when the DWT is applied to the LSN matrix. After converting the 4-bit RSN into decimal values between 0 and 15, the RSN matrix is subjected to HOG in order to provide a second set of spatial domain characteristics. Spatial and transform domain features undergo linear convolution to get the final features. The pictures are categorized using an Artificial Neural Network (ANN).

Face recognition using Wavelet and Fourier transformations was introduced by Zhao Lihong et al. [20]. The Nearest-Neighbor classifier uses the correlation coefficient and Euclidean distance as comparison metrics to classify the features, which are discovered by combining DWT with the Fourier transform. A biometric face identification technique based on frontal face photographs that combines the wavelets theory with the structure of probabilistic neural networks was presented by Espinosa-Duro and Monte-Moreno [21]. A radial basis neural net classifier is utilized for the identification step after the DWT reduces the dimensionality of the facial images. By introducing additive white Gaussian noise to the test photos in the face database, Atamuradov et al. [22] examined the effectiveness of the suggested technique. DWT and Dual-Tree Complex are the two algorithms. For de-noising, Wavelets Transform (DTCWT) is employed. For better outcomes, PCA-based face recognition is then applied to the de-noised images. As a preprocessing for face recognition, Lahaw et al. [23] took advantage of the concept of 2D-DWT for image compression. For sensitivity to changing lighting conditions and facial nuances, the DWT is performed at several scales and placements. The ICA, PCA, LDA, and SVM algorithms are utilized to extract features from the processed image's LL sub-band.

Proposed System Model

This section covers facial image-based human recognition by cascading previous methods, such as DWT and HOG. The next steps construct the experimental setup to use convolution to fuse the input and outputs of the HOG algorithm to extract robust features.

Image datasets
Four standard face data sets—JAFFE, L-SPACEK, YALE, and ORL—are used to test the suggested model.

Japanese Female Face Expression (JAFFE)
It includes ten unique individuals, each with twenty different photographs, for a total of 200 image samples. Each image has a grayscale resolution of 256 × 256. The database photos were taken in a frontal, upright stance. Figure 1 displays all of the tiff-formatted photos of a single individual with seven distinct emotive face expressions.

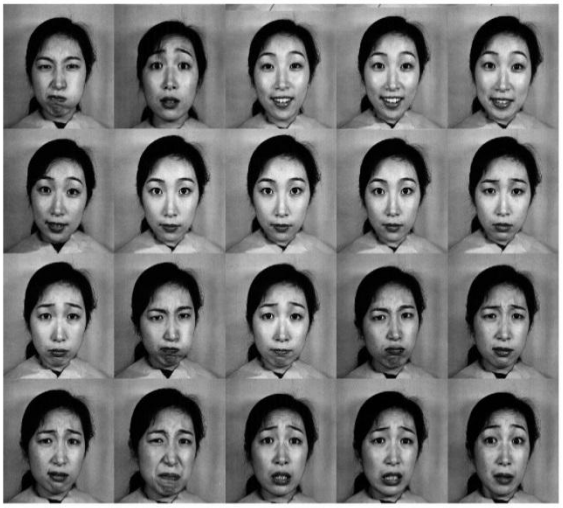

Figure 1. Images of JAFFE data set [24]

Libor Spacek's (L-Spacek's) Facial Images Databases

There are 20 photos of each of the 152 people in the collection, totalling 3040 photos. Only face expressions are different in all the photographs, which are 200X180 24-bit GRB images with a plain green background. Twenty face image samples of a single person are displayed in Figure 2.

Figure 2. Twenty L- Spacek's Samples of one person [25]

YALE Database
The collection consists of 3040 photographs, with 20 images of each of the 152 individuals. All the photos are 200X180 24-bit GRB images with a basic green background, and the only differences are in the expressions on the faces. Figure 3 shows samples of a single person's face picture.

Figure 3. Images of Yale database [26]

ORL Database

Pictures taken between 1992 and 1994 are included in a standard Olivetti Research Laboratory (ORL) face database. A single person's 10 distinct facial expressions—such as open or closed eyes, smiling or not, wearing or not wearing spectacles, and varied lighting conditions—are recorded. In a similar manner, forty people's faces were photographed in various settings. When taking pictures, a shaded background, an upright frontal, and a slight head tilt are taken into account. There are 400 pictures of 40 people in all, all in PGM format, and each one is 92 by 112. Figure 4 displays ten images of a single person.

Figure 4. ORL samples of single person [27]

Preprocessing

For quick and easy image processing, the RGB face images are transformed to grayscale. To extract a fixed number of features for all types of face databases, the grayscale images from several benchmarked face image databases with varying dimensions are shrunk to a standard dimension of 128×128.

Discrete Wavelet Transform (DWT)

Applications include finding pure frequencies, compressing pictures, de-noising signals, and extracting biometric trait information. Face picture compression and de-noising are two uses for this process. The basis function wavelet is scaled and shifted in this linear transformation. The wavelet is a tiny wave with an average value of zero and a finite duration. By combining time and frequency information, the wavelet transform gets beyond the drawbacks of other transformations. The wavelet's energy is evenly distributed in both positive and negative directions, and its window width varies. Using Low Pass Filter (LPF), High Pass Filter (HPF), and down sampling of image rows and columns, Figure 5 illustrates its band pass characteristics in the frequency domain.

Sub-band coding is used to execute the 2D-DWT signals for computerized images. With the use of sub-band examination, images are extracted in approximate shapes in both horizontal and vertical headings, facts in horizontal headings to find horizontal edges, specifics in vertical headings to find vertical edges, and specifics in both horizontal and vertical headings to find diagonal edges. According to taking after circumstances, the 2-D signal analysis uses taking over 2-D filter tasks to finish the rise of discernible scaling and wavelet tasks in n1 tests in horizontal headings and n2 tests in vertical headings [28].

Each sub-band corresponds to one-fourth of the input dimensions, and the sub-sampling filter is multiplied by two. LL, LH, HL, and HH are the respective designations for the sub-bands φ (n1, n2), Ψ^{H} (n1, n2), ΨV (n1, n2), and Ψ^{D} (n1, n2).

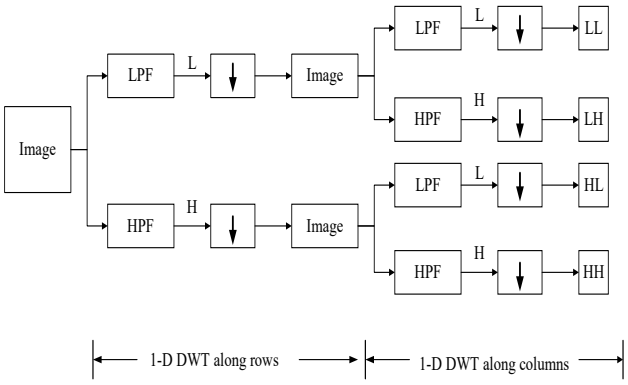

Figure. 5 One level 2D-DWT image decomposition

The LL band is an approximation band that has low frequency components and carries a substantial amount of information about the original image. The detailed bands that correspond to high frequency components are LH, HL, and HH. LH, HL, and HH, respectively, provide the horizontal, vertical, and diagonal edge information that adds a little bit of information to an original image. The primary 128 x 128 image is divided into four sub-bands, each measuring 64 x 64 pixels. Our technique uses only 64x64 LL band coefficients.

Histogram of Oriented Gradient (HOG)
Because it works with local matrix cells, it may be detected by humans in face photos and is resistant to changes in geometry and photometry [29, 30, 31]. The HOG of the LL Sub-band is calculated by the following kernels, dx and dy, utilizing vertical and horizontal gradients.

$dx = [-1\ 0\ 1]$
$dy = [-1\ 0\ 1]^T$

For LL band matrix I, the gradients can be computed using convolution operation as given in Equations below.

$I_x = I * dx$
$I_y = I * dy$

The gradient magnitude and directions are calculated using the Equations shown.
Magnitude of gradient $= \sqrt{\mathrm{Ix2} + \mathrm{Iy2}}$
Angle of gradient = $\arctan \frac{I_y}{I_x}$

The LL band matrix is divided into 8×8 pieces to calculate the HOG of the LL band matrix. The angles are unsigned gradients since their negative values are represented by identical numbers, and they range from 0 to 180 degrees rather than 0 to 360 degrees for an 8x8 matrix. illustrates the procedure for determining the size and orientation of the HOG gradient for the 8X8 region. The value is filled with the magnitude, and the bin is chosen according to the direction.

Directions 0, 20, 40, 60, 80, 100, 120, 140, and 160 are represented by the 9-bin histogram that is created by combining all of the coefficients in the 8X8 cells. The magnitude determines the value that goes into the bin, and the angle determines which bin is chosen. The fifth bin corresponds to the coefficient value circled in blue, which has an angle of 80 degrees and a corresponding magnitude of 2. The gradient at the red-circled coefficient has a magnitude of 4 and an angle of 10 degrees. Given that 10 degrees is halfway between 0 and 20, the mapping divides equally into the first and second bins. The 9-bin histogram is obtained by adding the histogram of gradients of each of the coefficients in the 8x8 cells. A 16x16 block with four 8x8 cells is utilized for normalization, yielding a 9x4=36×1 feature vector. To lessen the impact of changes in the illumination of the original face photos, the L2-Norm of normalization is applied to the 39x1 histogram gradient vector from the 16x16 matrix of the LL band. Since there are seven overlapping 16x16 (8x8) blocks in the 64x64 LL band matrix, there are seven overlapping 7x7 features in total. Thus, the size of the feature vector is 1764 x 1. The HOG row histogram vector 1764×1 of LL is transformed into a matrix. Let $\mathrm{pi} = [\mathrm{p1}, \mathrm{p2}, \mathrm{p3}, ----\mathrm{pM}]$be the initial vector. A second vector of size 42×42, $\mathrm{qi} = [\mathrm{q1}, \mathrm{q2}, \mathrm{q3}, --------\mathrm{qM}]$, should be considered.

Convolution [33]

By reducing noise and improving edge detection and sharpening, the convolution between two sets of features—a combination of two feature types—produces a largely remarkable third set of characteristics for biometric recognition. It generates a new convolution result with a distinct output by adding the products of the LL band coefficients and HOG coefficients of the LL band after one is reversed and shifted. The summation is then assessed for all values of shift. The LL band matrix H (M2, N2) of size 42X42 and the LL band image L (M1, N1) of size 64X64 are convolved. Equation below provides the last aspects of the face image.

$F(u,v) = \sum_{m=0}^{M_1-1} \sum_{n=0}^{N_1-1} L(m,n) \cdot H(u-m, v-u)$
Where,$0 \le u \le (M_1 + M_2 - 1)$ and $0 \le v \le (N_1 + N_2 - 1)$

Matching [34]

The Euclidean Distance (ED) is the computation of distance between two points in two vectors to compare similarities and differences between two vectors and is given in Equation.

Let first vector $pi = [p1, p2, p3, - - - - - pM]$
Let second vector $qi = [q1, q2, q3, - - - - - - - qM]$

$$D1(p,q) = \sqrt{\frac{1}{M}\sum_{i=1}^{M}(pi - qi)^2}$$

In this case, M represents the feature vectors' dimension, pi represents the database feature vector's coefficients, and qi represents the test feature vector's coefficients.

Proposed Algorithm
The problem definition is human recognition utilizing face images, with initial features extracted using cascading DWT and HOG. To assess the system's performance, the HOG's input and output are convolved to extract reliable final features. The system's objective is to extract reliable facial image attributes from a range of image variants. The system's goal is to identify people with 1. A high recognition rate 2. Minimal rate of errors. Input: The suggested model is tested using standard face databases. Output: To confirm the superiority of the system, the performance parameters are calculated.

Step 1: Consideration is given to face databases such JAFEE, L-Space K, YALE, and ORL.
Step 2: RGB to grayscale face image conversion is done using a pre-processing technique, and various face databases' dimensions are changed to a standard 128x128 size.
Step 3: To create low (LL) and high frequency bands, DWT is applied to the previously processed image.
Step 4: To create a 42x42 HOG matrix, HOG is applied to the LL band (64x64) of DWT.
Step 5: A cascade connection is made between the DWT and HOG. The final robust features are produced by convolving the 64x64 input and 42x42 output of HOG.
Step 6: Performance metrics for comparing database features and test image features are determined using the distance formula ED.
Step 7: By building databases with various Persons Inside Database (PID) and Persons Outside Database (POD) combinations, the system's performance is assessed.
Step 8: To demonstrate the superiority of the suggested approach, the system performance is contrasted with that of current approaches.

Proposed model implementation and analysis
Performance metrics, experimental analysis with four face data sets, and a comparison of the suggested model with current approaches are covered in this part. For various combinations of Person Inside Database (PID) and Person Outside Database (POD), the values of FAR, FRR, EER, MTSR, and OTSR are calculated and the fluctuations regarding the threshold values are plotted.

Performance Metrics
False Accept Rate (FAR)
The images in the data set match the test image, which is not part of the data set. Equation can be used to compute the FAR.

$$FAR = \frac{Number\ of\ imposter\ person\ accepted\ genuine}{Total\ number\ of\ persons\ outside\ the\ database}$$

False Rejection Rate (FRR)

The test image from the data set is not matched with the images in the data set and can be calculated using Equation.

$$FRR = \frac{Number\ of\ genuine\ persons\ in\ the\ database\ rejected}{Total\ number\ of\ persons\ inside\ the\ database}$$

Equal Error Rate (EER)

It is the juncture value of FRR and FAR in the graph.

Recognition Rate (RR)

The number of legal persons successfully matched in the data set and is given by Equation 13.

$$TSR = \frac{Number\ of\ genuine\ persons\ recognized\ correctly}{Total\ number\ of\ persons\ inside\ the\ database}$$

Maximum RR (MRR)

The maximum value of RR.

Optimum RR (ORR)

The RR value corresponding to EER value.

Implementation and Experimental Result Analysis

The suggested model is evaluated using performance metrics on the face datasets JAFFE, L-SPACEK, YALE, and ORL. To calculate FRR and FAR for the assessment of percentage RR, the entire population in the dataset is divided into two groups, Persons Inside Database (PID) and Persons Outside Database (POD).

Result Investigation using JAFFE DataSet

Each of the ten people in this collection has twenty photographs. For variances in threshold values, the performance indicators—such as % FRR, FAR, and TSR—are plotted. For combinations of 4:4, 5:4, and 6:4, the variations of FRR, FAR, and TSR were calculated for PID deviations with constant POD, correspondingly. For 5:4 and 6:4 combinations, the variations of FRR, FAR, and TSR were calculated for constant PID with POD deviations, respectively. It has been noted that as threshold values increase, FRR values decrease, but FAR and TSR values increase.

Table 1 prepares the % EER, OTSR, and MTSR values for various PID and POD mixes. It is observed that the percentage of OTSR values increases as PID values increase, but the percentage of MTSR values remains constant at 100.

Table 1. Deviations of result METRICS with PID and POD for JAFFE Database

PID	POD	%EER	%OTSR	%MTSR
4	4	15	75	100
5	4	14	80	100
6	4	12	84	100
4	5	15	75	100
4	6	12	75	100

Result Investigation using L-SPACEK Dataset

This dataset contains a total of 152 individuals, each of whom received 20 photos. The parameters—FRR, FAR, and TSR—are plotted after being computed for deviation using threshold values. the differences between constant POD and PID deviations in terms of FRR, FAR, and TSR. 40:60, 50:60, and 60:60 are the comparable combinations. The percentage FRR, FAR, and TSR deviations were calculated for constant PID with POD deviations for 60:40 and 60:50 combinations, respectively. While the FAR and TSR values increase as the threshold values climb, the observed FRR values decrease as the threshold values grow. TSR values decline from 100% to 0% for threshold values below 0.6, while they remain constant

at 100% of the threshold values between 0.6 and 1.2. The TSR values stay the same for higher threshold values, however the FAR values rise from 0% to 100%, which is a drawback.

Table 2 lists the variations in EER, OTSR, and MTSR values for different PID and POD amalgamations.

Table 2. The result constraints with different PID and POD combinations for L-SPACEK.

PID	POD	%EER	%OTSR	%MTSR
40	40	0	99	100
40	50	0	99	100
40	60	0	98	100
50	60	0	99	100
60	59	0	99	100

Targeting the various PID and POD combinations for threshold values between 0.6 and 1.2, the computed EER, OTSR, and MTSR percentage values stay nearly consistent at 0, 99, and 100. The percentage MTSR is 100% for higher threshold values, which is advantageous; however, the percentage FAR rises to 100%, which is the most undesirable outcome.

Result Investigation using YALE Dataset

There are fifteen people in this collection, and each person has eleven photos. The graphs show the computed results of percentage FRR, FAR, and TSR for changes in threshold values. For combinations of 8:5, 9:5, and 10:5, the equivalent deviations of FRR, FAR, and TSR were obtained for PID deviations with constant POD. For combinations of 8:6 and 8:7, respectively, the deviations of FRR, FAR, and TSR produced were intended to maintain a constant PID with variations in POD. It is observed that when threshold values increase, FRR values decrease, however FAR and TSR values increase as threshold values grow. TSR values drop from 100% for threshold values less than two, while they remain constant at 100% for threshold values greater than two. The TSR values stay high and steady for higher threshold values, but the FAR values rise from 0% to 100%, which is a drawback.

Table 3 lists the EER, OTSR, and MTSR percentage values for various PID and POD combinations. For POD variations and constant PID combinations of threshold values closer to 1.9, it is seen that the percentage values of EER and OTSR stay constant at 12 and 88, respectively. The percentage MTSR is 100% for threshold values greater than 2, which is advantageous; nevertheless, the most unpleasant situation is when the percentage FAR increases as the threshold rises to 100%.

Table 3. The result constraints with different PID and POD combinations for YALE

PID	POD	%EER	%OTSR	%MTSR
8	5	12	88	100
8	6	12	88	100
8	7	12	88	100
9	5	11	89	100
10	5	10	90	100

Result Investigation using ORL Dataset

Each of the 40 unique individuals in the collection has 10 different photos. For variances in the threshold values, the performance metrics—FRR, FAR, and TSR—are computed and presented in the diagrams. For combinations of 10:10, 20:10, and 30:10, respectively, the deviations of FRR, FAR, and TSR were obtained for variances in PID with constant POD. For combinations of 10:20 and 10:30, the FRR, FAR, and TSR deviations were calculated for constant PID with POD deviations, respectively. While the FAR and TSR values increase through threshold levels, the FRR values decrease as threshold values increase. At 100% of the threshold values from 2.1, the TSR value remains constant; however, for threshold values below 2.1, the TSR value drops from 100% to 0%. The TSR values stay constant at high threshold values, while the FAR values rise from 0% to 100%, which is a drawback.

Table 4 lists the differences in the percentage values of EER, OTSR, and MTSR for different PID and POD mixes. For POD changes and constant PID combinations of threshold values about 1.7, the % EER and OTSR values are nearly constant at 20 and 80, respectively. The percentage MTSR is 100% for threshold values greater than 2.2 with constant PID at 10, which is advantageous; nevertheless, the most unpleasant situation is when the percentage FAR increases as the

threshold rises to 100%.

Table 4. The result constraints with different PID and POD combinations for ORL

PID	POD	%EER	%OTSR	%MTSR
10	10	20	80	100
10	20	20	80	100
10	30	18	80	100
20	10	15	75	85
30	10	20	74	86

Comparison of results using different face datasets

The L-Spacek, YALE, JAFFE, and ORL face datasets are used to record the performance measures EER and OTSR that correspond to threshold values (Table 5). Since there are very few differences in the face photos of different people, it is observed that for lower threshold values, the quarry face images match the dataset face images (prestored), and the EER and OTSR for the L-Spacek dataset are zero and 99%, respectively. For face datasets, such as YALE, JAFFE, and ORL, high threshold values are needed to match query and dataset photos. Because each person's stance and other facial image variances are high, the average EER values are high while the average OTSR values are low.

Table 5. Comparison of results for different datasets

Metrics	Face Datasets			
	L-Spacek	YALE	JAFFE	ORL
Average Threshold	0.5	1.8	1.4	1.75
% Average EER	0	11.4	13.5	19
% Average OTSR	99	89	77.5	77.8

Comparison of Projected Technique with Current Techniques

Table 6 displays the percentage MTSR utilizing the ORL, YALE, and JAFFE face datasets of the projected technique in relation to the present methods obtained by Yubo Wang et al., [37], Shailaja and Anuradha, [36], and Erhu Zhang et al., [35]. According to the comparison, the anticipated technique's percentage MTSR is higher than that of the present methods.

Table 6. %MTSR Comparison of Projected Technique with Current Approaches

Methods	%MTSR		
	ORL dataset	YALE dataset	JAFFE dataset
Erhu Zhang et al.,[35]	74.06	80.77	-------
Shailaja and Anuradha[36]	87	92.8	-----
Yubo Wang et al.,[37]	----	-----	92.4
Projected method	94.2	100	100

3. CONCLUSION

This research proposes a Convolution of Hybrid Domain Features for Human Recognition from Face Images. A consistent form dimension of 128x128 is created from the face photographs of various face databases with varying dimensions. By considering the low frequency coefficients of the LL band, the DWT is used to compress and eliminate noise from face photographs. A cascade link between DWT and HOG is the outcome of normalizing the HOG using L2-Norm from the LL band. Using a convolution approach, the 64x64 LL band matrix is merged with a 42x42 HOG reshaped matrix to produce effective and reliable final features for face images. The result constraints are measured using the ED approach. It is observed that the suggested method outperforms the current facial recognition methods. Large image collections can be

compared in the future using deep learning approaches instead of ED.

REFERENCES

[1] B. Miller, “Vital Signs of Identity,” IEEE Spectrum, vol 31, issue 2, pp 22–30, 1994.
[2] G. Lawton, “Biometrics: A New Era in Security,” Industry Trends, IEEE Computer, vol 31, pp16-18, 1998.
[3] A. Jain, R. Bolle and S. Pankanti, Biometrics: Personal Identification in Networked Society, Kluwer Academic Publishers, 1999
[4] D. Zhang, Automated Biometrics Technologies and Systems, Kluwer Academic Publishers, 2000
[5] E. C. Titchmarsh, Introduction to the Theory of Fourier Integral, Oxford University Press, NY, 1948
[6] Steven W. Smith, in Digital Signal Processing: A Practical Guide for Engineers and Scientists, Science Direct, 2003.
[7] J. W. Cooley, P. A. W. Lewis and P. D. Welch, “Historical Notes on the Fast Fourier Transform,” IEEE Transactions on Audio and Electroacoustics, Vol 15, issue2, pp 76–79,1967.
[8] J. W. Cooley, P. A. W. Lewis and P. D. Welch, “Application of the fast Fourier transform to computation of Fourier integrals,” IEEE Transactions on Audio and Electroacoustics, Vol 15, issue2, pp 79–84,1967.
[9] Vladimir Britanak, Patrick C. Yip and K.R. Rao, Discrete Cosine and Sine Transforms General Properties, Fast Algorithms and Integer Approximations, ScienceDirect, 2006
[10] Ali N. Akansu, and Richard A. Haddad, in Multiresolution Signal Decomposition (Second Edition), ScienceDirect, 2001
[11] X. Han, Q. Liu, J. Xu and H. Chen, "Face Recognition using Pearson Correlation and HOG with Single Training Image Per Person," IEEE Conference on Chinese Automation Congress (CAC), pp. 3294-3298, 2018.
[12] G. G. Rajput, Prashantha and B. Geeta, "Face Photo Recognition from Sketch Images using HOG Descriptors," IEEE Second International Conference on Inventive Communication and Computational Technologies (ICICCT), pp. 555-558, 2018.
[13] Z. Xie, P. Jiang and S. Zhang, "Fusion of LBP and HOG using multiple kernel learning for infrared face recognition," IEEE/ACIS International Conference on Computer and Information Science (ICIS), pp. 81-84, 2017.
[14] M. Ghorbani, A. T. Targhi and M. M. Dehshibi, "HOG and LBP: Towards a Robust Face Recognition System," IEEE Tenth International Conference on Digital Information Management (ICDIM), pp. 138-141, 2015.
[15] H. Wang, D. Zhang and Z. Miao, "Fusion of LDB and HOG for Face Recognition," IEEE 37th Chinese Control Conference (CCC), pp. 9192-9196, 2018.
[16] H. T. M. Nhat and V. T. Hoang, "Feature Fusion by using LBP, HOG, GIST Descriptors and Canonical Correlation Analysis for Face Recognition," IEEE 26th International Conference on Telecommunications (ICT), pp. 371-375, 2019.
[17] B. H. Prasetio, H. Tamura and K. Tanno, "The Facial Stress Recognition Based on Multi-Histogram Features and Convolutional Neural Network," IEEE International Conference on Systems, Man, and Cybernetics (SMC), pp 881-887, 2018.
[18] C. Jain, K. Sawant, M. Rehman and R. Kumar, "Emotion Detection and Characterization using Facial Features," IEEE 3rd International Conference and Workshops on Recent Advances and Innovations in Engineering (ICRAIE), pp. 1-6, 2018.
[19] P Rangsee, K B Raja and K R Venugopal, "Nibble-Based Face Recognition using Convolution of Hybrid Features," IEEE International Conference on Imaging, Signal Processing and Communication (ICISPC), Singapore, pp. 112-116, 2019.
[20] Zhao Lihong, Tian Yanan and Zhang Xili, "Face Recognition based on Wavelet and Fourier Transform," IEEE Chinese Control and Decision Conference, pp. 4225-4229, 2008.
[21] V. Espinosa-Duro and E. Monte-Moreno, "Face Recognition Approach based on Wavelet Transform," 42nd Annual IEEE International Carnahan Conference on Security Technology, pp. 187-190, 2008.
[22] V. Atamuradov, A. Eleyan and B. Karlik, "Performance Evaluation for Face Recognition using Wavelet-based Image De-noising," IEEE The International Conference on Technological Advances in Electrical, Electronics and Computer Engineering (TAEECE), pp. 284-287, 2013.
[23] Z B Lahaw, D Essaidani and H Seddik, "Robust Face Recognition Approaches using PCA, ICA, LDA Based on DWT, and SVM Algorithms," IEEE 41stInternational Conference on Telecommunications and Signal Processing (TSP), pp. 1-5, 2018.
[24] Micheal J Lyons, “The Japanese Female Face Expression (JAFFE) Database”, 1998, http://www.karsl.org/jaffe.html.
[25] L-spacek databasehttp://cswww.essex.ac.uk/mv/allfaces.
[26] Yale University, “The Yale Face Database”, 1997”, http://cvc.cs.yale.edu/cvc/projects/yalefaces/yalefaces.html
[27] AT&T Laboratories Cambridge, “The ORL Database of Faces”, 1994, http://www.cl.cam.ac.uk/research/dtg/attractive/face database.htm.

[28] Multi-resolution Analysis: Discrete Wavelet Transforms, https://nptel.ac.in/content/storage2/courses/117105083/pdf/ssg_m4l12.pdf.
[29] N. Dalal and B. Triggs, “Histograms of Oriented Gradients for Human Detection,” IEEE Computer Society Conference on Computer Vision and Pattern Recognition, pp 886–893, 2005.
[30] N. Dalal and B. Triggs, “Human Detection using Oriented Histograms of Flow and Appearance”, Springer-Verlag, LNCS European Conference on Computer Vision, pp 428-441, May 2006.
[31] HOG:Computation https://www.learnopencv.com/histogram-of-oriented-gradients/
[32] S. A. Korkmaz, A. Akçiçek, H. Bínol and M. F. Korkmaz, "Recognition of the stomach cancer images with probabilistic HOG feature vector histograms by using HOG features," IEEE 15th International Symposium on Intelligent Systems and Informatics (SISY), pp. 339-342, 2017.
[33] C M Rader, "Discrete Convolutions via Mersenne Transforms," IEEE Transactions on Computers, vol. C-21, no. 12, pp. 1269-1273, December 1972.
[34] Anton, Howard (2014), Elementary Linear Algebra (11th ed.), John Wiley & Sons. Erhu Zhang,
[35] Yongchao Li and Faming Zhang, “A Single Training Sample Face Recognition Algorithm Based on Sample Extension”, 2013 Sixth International Conference on Advanced Computational Intelligence, pp. 19-21, 2013.
[36] K. Shailaja and B. Anuradha, “Effective Face Recognition using Deep Learning Based Linear Discriminant Classification”, IEEE International Conference on Computational Intelligence and Computing Research, pp. 1- 6, 2016.
[37] Yubo Wang, Haizhou AI, Bo WU and Chang Huang, “Real Time Facial Expression Recognition with Adaboost”, IEEE International Conference on Pattern Recognition, pp. 926-929, 2004.